Estimation of Cell Traction and Migration in an Isometric Cell Traction Assay

David M. Knapp, Theodore T. Tower, and Robert T. Tranquillo
Depts. of Chemical Engineering and Materials Science, and Biomedical Engineering, University of Minnesota, Minneapolis, MN 55455

Victor H. Barocas
Dept. of Chemical Engineering, University of Colorado, Boulder, CO 80309

A quantitative analysis of data from an in vitro assay presented allows for simultaneous study of cell migration within as well as cell traction on tissue equivalents (collagen gels seeded with tissue cells to serve as model tissues). Using our anisotropic biphasic theory for modeling tissue equivalents, the ability of the model to simulate the data was validated by accurately predicting the alignment of fibroblasts and collagen fibrils in the compacting collagen gels and the effects of gel aspect ratio on gel compaction. The effects of migration and adhesion modulating factors (platelet-derived growth factor-BB and an anti-β_1 integrin antibody), as well as mechanical stress in the collagen network (attached vs. floating gels), on cell migration and traction during compaction were investigated. In all cases, cell migration was negatively correlated with cell traction. The relevance of the results to wound contraction is discussed.

Introduction

The mechanical interaction of tissue cells with fibrils in the surrounding extracellular matrix (ECM) is fundamental to cell behavior in native soft tissues and biopolymer gels, and thus to many problems spanning biology to tissue engineering. The most relevant biopolymer gels are collagen and fibrin gels, which are highly hydrated networks of entangled protein fibrils (more than 99% cell culture medium when the gel forms), and are used as models for normal tissue and early wound tissue, respectively. Examples of cell-ECM mechanical interactions include basic studies of cell behavior and tissue remodeling (Bell et al., 1979; Grinnell and Lamke, 1984; Tuan et al., 1996), tissue morphogenesis (Murray et al., 1983; Oster et al., 1983), wound contraction (Olsen et al., 1995; Tranquillo and Murray, 1992), and the fabrication of ''tissue-equivalents'' (TEs) based on entrapment of tissue cells within forming biopolymer gels (Barocas et al., 1998; Barocas and Tranquillo, 1997a; L'Heureux et al., 1993). In each of these examples, the ability of cells to exert traction on the ECM leading to local reorganization of ECM fibrils and macroscopic deformation of the tissue is central.

Wound contraction is of particular relevance to this study since it inherently involves cell migration as well as cell traction; the cells (wound fibroblasts) that generate the force for wound contraction must migrate into the wound from the surrounding tissue. While there is no doubt that cell traction is necessary for cell migration, there is as yet no direct evidence demonstrating that cell migration generates the force for wound contraction, although this has been suggested based on circumstantial evidence (Ehrlich and Rajaratnam, 1990) and often speculated (for example, Gross et al., 1995).

Cells mainly use adhesion receptors (integrins) on the cell surface in order to adhere to the ECM. Interestingly, while adhesion-dependent traction appears necessary for migration of neutrophils (the white blood cell that predominates in acute inflammation that precedes wound healing) on a surface, adhesion does not appear necessary for the traction facilitating its migration within a gel (Brown, 1982; Schmalstieg et al., 1986). Traction in a gel might be attained by purely mechanical means, such as a (nonadhering) pseudopod that extends between and around fibrils providing numerous points of anchorage (traction) when the pseudopod attempts to retract (Lackie, 1986). It is unknown to what extent fibroblast migration in a tissue is integrin-mediated and how this relates to

Correspondence concerning this article should be addressed to R. T. Tranquillo.

cell traction that is prerequisite for migration and tissue contraction. However, the β_1 integrins have been identified to mediate the compaction of collagen gels by fibroblasts (Carver et al., 1995), a process in which cells entrapped in the gel contract the fibrillar network and cause the interstitial cell culture medium to exude—a cell induced gel syneresis.

While we and others have developed *in vitro* assays and methods to quantify fibroblast migration *or* traction in collagen and fibrin gels, no study has been reported in which both migration *and* traction have been quantified simultaneously. Cell tracking in a compacting gel and the track analysis are more complicated than on a rigid surface because of the convective movement of the cell with the network. An approach is described here which combines our ability to track cells in nonconvecting gels (Dickinson et al., 1993, 1994), adapted to account for cell convection due to gel compaction, with our ability to measure cell traction via gel compaction (Barocas et al., 1995), adapted to a geometry that facilitates a comparison of floating and attached gels. The comparison of floating and attached gels is of interest because the development of mechanical stress that occurs in an attached gel, due to the mechanical constraint opposing cell traction, results in dramatic differences in DNA and protein synthesis (Mochitate et al., 1991). Whether differences exist in cell migration and traction between floating and attached gels is unknown.

The isometric force developed in a TE that is anchored at both ends has been measured using a force transducer (Delvoye et al., 1991; Kolodney and Wysolmerski, 1992; Eastwood et al., 1994). We refer to this as an isometric cell traction assay (ICTA). Our approach to the ICTA reported here, in contrast, is based on measuring the compaction and associated cell and fibril alignment that develops in a TE cylinder attached at both ends using time-lapse video microscopy. This enables us to estimate the value of a cell traction parameter τ_0 from these data using our anisotropic biphasic theory (ABT) of TE mechanics that we developed to describe the mechanics of generic TEs (Barocas and Tranquillo, 1997a) and apply to model the ICTA (Barocas and Tranquillo, 1997b). τ_0 is a parameter that appears in the active stress term of the stress tensor for the network phase in its momentum conservation equation which models traction exerted by cells on the network fibrils. The estimation of τ_0 is possible, because we have characterized the viscoelasticity and permeability of collagen gel (Knapp et al., 1997) and the other relevant aspects of cell behavior in such assays of cell traction like the ICTA, namely proliferation (Barocas et al., 1995) and migration (Dickinson et al., 1994).

In Barocas and Tranquillo (1997b), it was shown that proliferation, as measured by a ''first-order proliferation rate constant'' k_0 and migration, as measured by a ''cell diffusion coefficient'' $\mathfrak{D}_0$, did not occur to a significant extent during the time-scale of TE compaction in terms of affecting the estimation of τ_0. While cells clearly need to exert traction in order to migrate, the ABT assumes τ_0 and $\mathfrak{D}_0$ are independent parameters. Although $\mathfrak{D}_0$ does not affect the estimation of τ_0, a goal of this study was to compare independent estimates of $\mathfrak{D}_0$ (from direct cell tracking during gel compaction) and τ_0 (from gel compaction) in the ICTA to assess if a correlation between migration and traction exists.

We have previously applied the ABT to floating TE spheres to estimate τ_0 and its dependence on the initial cell concentration c_0 (Barocas et al., 1995), revealing τ_0 increased with c_0 presumably due to one or more stimulatory autocrine factors released by the human foreskin fibroblasts used. The ABT predicts that floating TEs retain their initial isotropic orientation of fibrils (Barocas et al., 1995) or evolve to an isotropic state if prealigned by an external field (Barocas et al., 1998), unlike mechanically constrained TEs such as in the ICTA where fibrils align along the axis of the TE cylinder due to the constraint at both ends. Thus, even if cell migration was occurring to a significant extent during compaction of the floating TE (no simultaneous cell tracking was performed in the Barocas et al., 1995 study), it should not result in a change from the initial homogeneous distribution of cells. That is because fibrils through which cells migrate are predicted to be randomly oriented, as has been subsequently confirmed experimentally (Bromberek et al., 1999). Another consequence of random cell orientation associated with the isotropic state of a floating TE is that the stress on the collagen network due to cell traction is isotropic. For floating TEs of sufficiently small dimension, as used in our studies, the total network stress is not only isotropic but also negligible. The only body force acting on the network associated with interstitial flow of solution through the network is negligible, meaning the total stress is independent of position in the TE. This fact, in conjunction with the stress-free condition at the free surface of floating TEs, supports the assertion of negligible stress in floating TEs (Barocas and Tranquillo, 1994).

While the axial bias in cell *migration* due to a contact guidance response to axial fibril alignment in the ICTA was predicted by Barocas and Tranquillo (1997b) not to significantly affect the initial homogeneous distribution of cells (and thus the estimation of τ_0), the axial bias in cell *alignment* was predicted to have a major effect. This is because aligned cells would exert traction with axial bias, whereas traction is inferred from radial compaction. The ABT uses a tensor to describe the local alignment distribution of fibrils, which is assumed to be directly related to the local deformation ellipsoid of the network. The direction of fibril alignment is assumed to be coincident with the major axis of the ellipsoid, which is normal to the direction of compression (the deformation ellipsoid for a floating TE is simply a sphere since the strain field is predicted to be isotropic). It also uses a tensor to describe the local alignment distribution of cells, which accounts for contact guidance by taking it to be a power κ of the tensor characterizing the fibrils, with κ being a contact guidance sensitivity coefficient. Thus, the prediction was that less radial compaction would be observed for cells having larger κ but with the same τ_0 because they would align strongly along the axis after only relatively small radial compaction during the ICTA (Barocas and Tranquillo, 1997b). The total stress in the network was predicted to vary with position, being compressive near the midplane where radial compaction is greatest, and tensile towards the ends where the TE is anchored. The effect of the TE aspect ratio in the ICTA was not considered in that theoretical analysis.

After describing our experimental methods and summarizing the ABT equations, we present fits of the ABT-based model on basic ICTA data, including maps of cell and fibril alignment as well as TE compaction and dependence on c_0 and aspect ratio. Since the ICTA inherently involves a mechanically constrained gel, these results only apply to fibro-

blast migration and traction with mechanical stress present. Thus, we also present results for a floating (stress-free) TE cylinder for comparison. Motivated by an unexpected correlation between $\mathfrak{D}_0$ and τ_0 found when changing the mechanical stress present in the TE, we also present results for the ICTA when increasing the concentration of a migration-stimulating soluble growth factor (platelet-derived growth factor-BB, PDGF-BB) (Enever et al., 1999) in the surrounding medium and when decreasing the presumptive number of integrins bound to collagen fibrils by adding an anti-β_1 integrin blocking antibody to the medium.

Materials and Methods

Cell culture

Rat dermal fibroblasts (RDF) were obtained from biopsies from healthy Fischer rats, and human foreskin fibroblasts (HFF) were obtained from neonatal foreskins. The procedure for isolation and harvesting for both cell types was essentially the same and has been reported previously (Freshney, 1987; Bromberek et al., 1999), so it will be described only generally here. The tissue was first treated with three washes of ethanol and chopped into small pieces. The resulting suspension was plated onto a six well plate and incubated for one week in Dubelco's modified essential medium (DMEM) (Gibco) supplemented with 20% fetal bovine serum (FBS) until fibroblasts predominated in the culture (verified by staining for procollagen-I). The fibroblasts were then passed by exposure to trypsin/EDTA in PBS (Gibco) for 10 min at 37°C and replating onto Petri dishes. After pass 3, the cells were collected after trypsin treatment and suspended in freezing compound. RDF and HFF were subsequently cultured through pass 10 in DMEM supplemented with 10% FBS with a fraction used for the assays described. Prior to each experiment, cells were removed from the Petri dish by trypsin treatment, washed twice with DMEM, and suspended in 0.5 mL Medium 199 (M199, Gibco). All cells used were between pass 3 and 10.

Preparation of collagen gels

Collagen gels were prepared as described previously (Knapp et al., 1997, 1999). Briefly, 20 μL of 1 M HEPES Buffer, 132 μL of 0.1N sodium hydroxide, 100 μL 10$\times$ MEM (Gibco), 60 μL M199, 1 μL Penicillin/Streptomycin (5,000 units of penicillin and 5,000 μg streptomycin/mL in 0.85% saline), 10 μL L-Glutamine (29.2 mg/mL in 0.85% saline), and 677 μL of Vitrogen 100 (Collagen Corp.) were combined cold to form 1 mL collagen solution at a collagen concentration of 2 mg/mL. Vitrogen 100 is 99% pepsin solubilized bovine type I collagen. Care was taken not to introduce bubbles into the collagen solution and the solution was warmed to room temperature just prior to use to prevent the formation of bubbles during the gelation process at 37°C.

Preparation of the ICTA and floating TE cylinders

The ICTA chamber consisted of a modified stainless steel ring (O.D. 2.5 cm, I.D. 1.5 cm, 0.6 cm thick) bounded on either side with glass (detailed below) within which the TE cylinder and incubation medium were contained. Two opposing 3 mm diameter holes bored through the side of the ring were located 1 mm from the bottom of the chamber to allow imaging through the TE cylinder using high magnification and relatively low working distance objectives. Two 3 mm diameter stainless steel rods (1.2 cm and 0.8 cm long, respectively) with flared ends were fit securely into the opposing holes. Porous polyethylene (Bel Art Products) disks also of 3 mm diameter and 1 mm thickness were pre-glued on to the ends of the rods with silicone adhesive (Dow Corning) to form the platens to which the TE cylinder would attach (shown in Figure 1). The opposing ends of the rods formed a gap across which the TE cylinder would be formed. The gap was chosen to be 4 mm unless indicated otherwise. A Teflon tube with inner diameter matching the diameter of the rods and two small holes (3 mm diameter) comprised a mold in which a collagen suspension was injected and an attached TE cylinder thus formed (the ends of the Teflon tube overlapped over the porous polyethylene platens and stainless steel by 1.5 mm so the collagen solution was contained within the tube). Silicon grease (Dow Corning) was used to seal the bottom of the chamber to a 22$\times$30 mm No. 1 cover slip prior to filling the ICTA mold.

The preparation of the ICTA is shown in Figure 1. Polystyrene beads (20 μm diameter, Polysciences) at a concentration of 2.5×10^4 beads/mL and cells at the designated cell concentration were suspended in the collagen solution using concentrated stock suspensions of each component. The collagen/bead/cell suspension was drawn into a 3 mL syringe fitted with a 23 gauge needle and injected into the Teflon tube. Once filled, the chambers were capped with a micro-

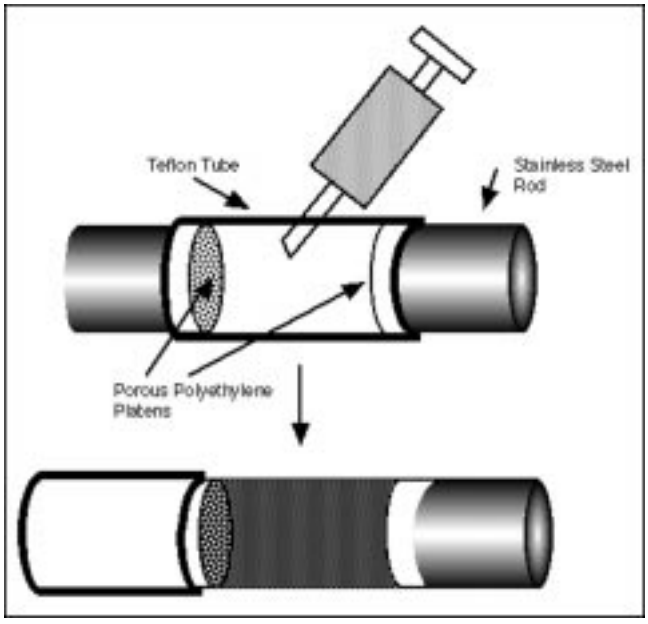

Figure 1. Preparation of the ICTA.

Polystyrene beads and fibroblasts were suspended in collagen solution and injected into the Teflon tube to form the TE in one step. The steel ring and coverslips comprising the chamber which housed the mold are not shown for clarity. The tube was slid over one steel rod and the resulting cylindrical TE, attached at both ends to the porous polyethylene platens, was incubated in cell culture medium resulting in a radial compaction of the free surface.

scope slide cut to the length of the chamber to minimize evaporation from the collagen solution. The chambers were then incubated for 45 min at 37°C to induce gelation of the collagen. The chambers were flipped every 5 min for the first half hour to ensure even distribution of beads and cells throughout the forming TE cylinder. After gelation, the chambers were filled with 1.25 mL of M199 supplemented with 10% FBS, 1% Penicillin/Streptomycin, and 1% L-Glutamine, along with added factors as dictated by the individual experiment (anti-β_1 antibody, Chemicon, or PDGF-BB, R&D Systems). Using sterile tweezers, the Teflon tube was removed by sliding it over the longer steel rod leaving the neutrally buoyant TE suspended between the two rods to which it was attached by the platens. The cut microscope slide was replaced on the top of the chamber using sterile silicone grease to seal the chambers. The chambers were then incubated at 37°C for the duration of the experiment.

Floating TE cylinders were prepared by filling cylindrical Teflon tubes (3-mm-ID, 4-mm-long) with the cell/collagen/bead suspension. The tubes were incubated for 45 min at 37°C and flipped periodically as for the ICTA. The resulting TE cylinders were carefully transferred into wells containing 1.25 mL M199 supplemented with 10% FBS, 1% Penicillin/Streptomycin, and 1% L-Glutamine and incubated prior to observation as for the ICTA.

Low magnification time-lapse observation of compacting tissue equivalents

Low and high magnification time-lapse video microscopy of the compacting TEs was conducted simultaneously using a Zeiss Axiovert 135 inverted microscope equipped with a motorized nosepiece allowing automated magnification changes. Images for the low magnification were acquired using a 2.5× objective and captured using a Hitachi KP-M2 CCD camera. A 2×2 mosaic image of the TE was taken at 45 min intervals and stored as a TIFF image. Compaction at the ICTA midplane was measured from this image by measuring the midplane diameter on each frame of the time lapse using the Inovision Isee image analysis software.

High magnification time-lapse observation for cell tracking

Tracks of migrating fibroblasts within the TE were generated using a modification of methods described earlier (Dickinson et al., 1994). Briefly, using a 40× objective, cells with obvious protrusions (that is, that were beginning to spread) were selected randomly from within the TE (at least 90% of the cells were spread at the end of the experiment in all samples reported). For both the HFF and RDF, the cell size was such that the cell extended across most of the field of view (95 μm×112 μm). Once the cells were selected and the time-lapse loop was initiated, the cells were focused using a software-based autofocus routine to adjust the z-position of the stage. Then, a series of image analysis routines were initiated to identify the cell centroid using Kontron IBAS image analysis software, and the x, y position of the stage was adjusted so that the cell centroid corresponded to the center of the field of view. The cell positions were updated at each time step by recording the x, y and z stage positions after recentering and autofocusing. The cell migration coefficient $\mathfrak{D}_0$ was determined using a generalized least-squares regression of the mean-squared displacement vs. time interval plot as described previously (Dickinson and Tranquillo, 1993). No attempt was made to resolve directional values of $\mathfrak{D}_0$ in order to account for contact guidance (Dickinson et al., 1994), so reported values include directional averaging.

The macroscopic compaction of the TEs resulted in a bias in the cell tracks in the direction of the local network convection. In order to account for this effect, the 20 μm polystyrene beads were co-entrapped with the cells in the collagen gel; the positions of beads near (within 400 μm) to the selected cells were tracked at the same time to approximate the local convection field. These bead tracks were subtracted from those of the corresponding cells to yield corrected cell tracks that were subsequently used in the analysis of migration in the TEs. Typically, 20 cells were tracked per sample.

Cell and fibril alignment measurements

Cell alignment during the ICTA was measured at 24 h after sample preparation (by alignment, we mean orientation in one of two opposite directions since the polarity of elongated fibroblasts typically cannot be determined from an image based on morphological criteria). Cell alignment was measured using previously described methods (Guido and Tranquillo, 1993). Briefly, the angle between the long axis of the cells observed using the 40× objective of the Zeiss microscope and the long axis of the TE cylinder α in the image was determined manually using Kontron IBAS image analysis software. The mean direction of alignment $\langle \alpha \rangle$ and strength of cell alignment $\Omega = \langle \cos^2 \alpha \rangle$ were determined and compared to ABT model predictions.

Fibril alignment was inferred during the ICTA from measuring the developing birefringence within the TE at low magnification (4× objective) in time-lapse. A methodology based on varying elliptically polarized light was used to determine the spatial dependence of birefringence (Tower and Tranquillo, 1999). The optic train on an Olympus IX-70 included the following elements in the order of the light path: a linear polarizer, a rotating quarter wave plate, the TE cylinder sample (automatically positioned by the Inovision software and motorized stages), a right circular analyzer, the 4× objective, and a Photometrics SenSys cooled CCD for image acquisition. The polarized light images were processed using Inovision DSP/OS image analysis software to determine the average direction and strength of collagen fibril alignment as a function of position within the TE cylinder. Although this method can generate a birefringence map with pixel resolution, results averaged over 12×6 pixels (400×200 μm) were sufficient to characterize the pattern of fibril alignment.

Data Analysis

The mechanical constraint that the platens imposed on the compacting TE cylinder resulted in nonuniform compaction and therefore led to fibril and cell alignment due to contact guidance. These effects were accounted for using our ABT developed for compacting TEs, which has been described extensively elsewhere (Barocas and Tranquillo, 1997a,b). Here, we give a brief description of the ABT and its application to modeling the ICTA.

The model consisted of five conservation equations (mass and momentum for network and solution and cell concentration) and three constitutive equations (cell alignment, network viscoelasticity, and cell spreading). The standard form of the conservation equations is presented here (Barocas and Tranquillo, 1997a). The ''Pressure Diffusion'' form actually solved for the ICTA model is presented in Barocas and Tranquillo (1997b). The mass conservation equations for the network and solution phases in terms of volume fractions θ_n and θ_s are

$$\frac{D\theta_n}{Dt} + \theta_n(\nabla\cdot\boldsymbol{v}_n) = 0 \tag{1}$$

$$\frac{D\theta_s}{Dt} + \theta_s(\nabla\cdot\boldsymbol{v}_s) = 0 \tag{2}$$

where $\boldsymbol{v}_n$ and $\boldsymbol{v}_s$ are the velocities of the phases and D/Dt denotes the substantial derivative moving with each phase. The momentum conservation equations for the solution and network are

$$\nabla\cdot\left[\theta_s(-PI)\right] - \varphi_o(\boldsymbol{v}_s - \boldsymbol{v}_n) = \mathbf{0} \tag{3}$$

$$\nabla\cdot\left[\theta_n(\boldsymbol{\sigma} + c\tau_0\boldsymbol{\Omega}_c - PI)\right] + \varphi_o(\boldsymbol{v}_s - \boldsymbol{v}_n) = \mathbf{0} \tag{4}$$

where P is the hydrostatic pressure, φ_0 is an interstitial drag coefficient between the network and solution phases, $\boldsymbol{\sigma}$ is the network viscoelastic stress tensor, τ_0 is the cell traction parameter, and $\boldsymbol{\Omega}_c$ is the cell alignment tensor that accounts for anisotropic cell traction stress when cells are aligned because network fibrils are aligned (that is, contact guidance). It can be deduced from Eqs. 3 and 4 that the solution is considered inviscid relative to the network which is about 10^8 times more viscous than the solution for the collagen gel used (Knapp et al., 1997).

Cell proliferation, convection, and anisotropic migration (as directed by contact guidance) were accounted for in the cell conservation equation as follows

$$\frac{Dc}{Dt} + c(\nabla\cdot\boldsymbol{v}_n) = \nabla\cdot(\mathfrak{D}_0\boldsymbol{\Omega}_c\cdot\nabla c) + k_0 c \tag{5}$$

where c is the cell concentration, $\mathfrak{D}_0$ is the cell migration coefficient, and k_0 is the rate constant for cell proliferation. Since the cells are considered a species in the network phase (in which they are convected and migrate and must attach for proliferation), the cell concentration is defined per unit volume of network phase and the substantial derivative is with respect to $\boldsymbol{v}_n$.

As mentioned previously, the cell alignment tensor $\boldsymbol{\Omega}_c$ is assumed to be a monotonically increasing function of the fiber alignment tensor $\boldsymbol{\Omega}_f$, which is determined by the deformation ellipsoid of the local strain field (Barocas and Tranquillo, 1997a)

$$\boldsymbol{\Omega}_c = \frac{3(\boldsymbol{\Omega}_f)^{\kappa}}{tr(\boldsymbol{\Omega}_f)^{\kappa}} \tag{6}$$

where κ is the cell contact guidance sensitivity parameter and the scalar prefactor ensures that $\boldsymbol{\Omega}_c = I$ when $\boldsymbol{\Omega}_f = I$. The strength of the cell alignment Ω defined previously is the 1,1 element of $\boldsymbol{\Omega}_c$.

Both shear (Moon, 1992) and compression (Knapp et al., 1997) experiments have demonstrated that the collagen network in TEs exhibits viscoelastic fluid behavior. Although it exhibits a spectrum of relaxation times (Knapp et al., 1997), for simplicity, the network was modeled using the single relaxation time compressible Maxwell fluid equation which has been shown to be of sufficient accuracy for compacting TEs up to about 15% strain (Barocas et al., 1995, 1998)

$$\frac{1}{2G}\dot{\boldsymbol{\sigma}} + \frac{1}{2\eta}\boldsymbol{\sigma} = \frac{1}{2}\left[\nabla\boldsymbol{v}_n + (\nabla\boldsymbol{v}_n)^T\right] + \frac{\nu}{1-2\nu}(\nabla\cdot\boldsymbol{v}_n)I \tag{7}$$

where G is the shear modulus, η is the shear viscosity, and ν is Poisson's ratio. The center dot denotes the upper-convected derivative.

In order to account for cell spreading and development of motility from an initial nonmotile spherical state when the TE is formed, the cell migration and traction stress coefficients were modified accordingly with a sigmoidal dependence on time (Barocas et al., 1995; Barocas and Tranquillo, 1994)

$$\mathfrak{D}_0(t) = \mathfrak{D}_0\frac{t^{(k_{sp})}}{t^{(k_{sp})} + \left(t_{1/2}\right)^{(k_{sp})}} \tag{8}$$

$$\tau_0(t) = \tau_0\frac{t^{(k_{sp})}}{t^{(k_{sp})} + \left(t_{1/2}\right)^{(k_{sp})}} \tag{9}$$

where k_{sp} determines the steepness of the spreading vs. time response and $t_{1/2}$ is the half time for cell spreading.

The boundary conditions for the symmetry plane and axis of the TE cylinder were as follows

$$v_n = (\boldsymbol{\sigma} + \tau_0 c\boldsymbol{\Omega}_c)_{nt} = \frac{\partial c}{\partial n} = \frac{\partial P}{\partial n} = 0 \tag{10}$$

where n and t refer to the normal and tangent directions. The boundary conditions for the free surface were

$$P = (\boldsymbol{\sigma} + \tau_0 c\boldsymbol{\Omega}_c)_{nn} = (\boldsymbol{\sigma} + \tau_0 c\boldsymbol{\Omega}_c)_{nt} = \frac{\partial c}{\partial n} = 0 \tag{11}$$

and, those for the platen allowed neither slip nor penetration

$$v_n = v_t = \frac{\partial c}{\partial n} = \frac{\partial P}{\partial n} = 0 \tag{12}$$

Fitting of the model to the compaction data was performed using an FEM solution of the above equations (for details see Barocas and Tranquillo, 1997b; Knapp et al., 1997). The parameter values used for the collagen gel material properties were obtained from confined compression experiments (Knapp et al., 1997) and the cell-related parameters $\mathfrak{D}_0$, k_0, κ, k_{sp}, and $t_{1/2}$ were determined as described previously (Barocas and Tranquillo, 1997a). The parameter values used

Table 1. ABT Parameter Values

Parameter	Parameter Value	Reference
Collagen Network		
Shear modulus G (dyne/cm^2)	11850	Knapp et al. (1997)
Shear viscosity η (dyne·s/cm^2)	1.24×10^{8}	Knapp et al. (1997)
Drag coefficient φ_0 (dyne·s/cm^4)	6.4×10^{6}	Knapp et al. (1997)
Poisson's ratio, υ (dimensionless)	0.2	Scherer et al. (1988)
Fibroblasts		
Contact guidance sensitivity parameter, κ (dimensionless)	4	Girton et al. (1999)
Migration coefficient $\mathfrak{D}_0$ (cm^2/s)	1.7×10^{-10}	Barocas et al. (1995)
Proliferation rate constant k_0 (s^{-1})	5.3×10^{-6}	Barocas et al. (1995)
Spreading steepness k_{sp} (dimensionless)	1.5—3.0	See Results
Spreading half time, $t_{1/2}$ (h)	3—5	See Results

in the fitting are shown in Table 1. As mentioned in the introduction, the values of $\mathfrak{D}_0$ and k_0 are so small they do not affect the estimation of τ_0, so a constant value of $\mathfrak{D}_0$ was used in all fits of the compaction data to estimate τ_0, even though $\mathfrak{D}_0$ was measured for each sample and varied among samples.

The compaction data fitted by the model were the midplane diameter as a function of time. The data were fit manually by varying τ_0, k_{sp} and $t_{1/2}$ (initial guesses for k_{sp} and $t_{1/2}$ were inferred from changes in the aspect ratio of cells observed at high magnification in time-lapse) until an acceptable fit was obtained. As explained in the Results section, the value of τ_0 required for an acceptable fit was not highly dependent on the values of k_{sp} and $t_{1/2}$. Since an optimizing code was not available for fitting the compaction data for our 2-D axisymmetric model of the ICTA as was used in parameter determination for a 1-D linear model for confined compression of collagen gel (Knapp et al., 1997), the accuracy of the simulation fits to the experimental data was tested by qualitative assessment of the sensitivity of the goodness-of-fit to the adjusted parameter τ_0. Figure 2 shows a typical ICTA compaction curve along with the best fit line and two bracketing lines in which the cell traction parameter has been varied by 5% on either side of the best fit value. Clearly, the best estimate for τ_0 lies within the two lines. Since the standard deviation for the best fit value of τ_0 for this experiment was approximately 10%, which was on the same order of magnitude as the error due to fitting, the values for the standard error among samples were reported and the error due to fitting was assumed to be small in comparison.

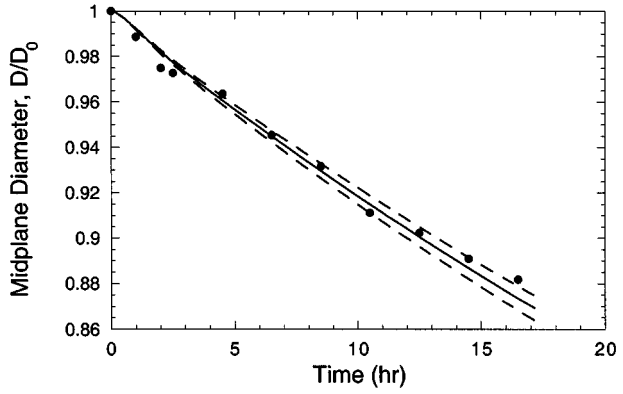

Figure 2. Uncertainty in fitting the cell traction parameter τ_0.

τ_0 was varied by $\pm5\%$, and the result is shown by the dashed lines in the figure. The variability due to the fit was less than the standard deviation between samples, and was neglected in the analysis.

Results of the effects of various treatments, such as PDGF-BB added to the incubation medium, were obtained for identically prepared samples in a single experiment (at least $n = 3$), with the experiment being repeated at least once. Significance relative to the mean for the control group was determined using Student's t-test. In order to exclude effects of variation in cell or collagen properties between experiments, the sensitivity of τ_0 estimated by data regression was determined with respect to the compression modulus and viscosity of collagen gel G_{cc} and η_{cc}, and to the cell contact guidance parameter κ. Since all the samples were prepared identically within a single comparison, using the same cells and collagen solution, the appropriate limits of the sensitivity are indicated by repeated tests on the same sample, which have been measured as 10% of G_{cc} and η_{cc} for collagen gel in confined compression (Knapp et al., 1997). The sensitivity of τ_0 to any of the parameters tested was not greater than 10%, which is less than the experimental variability between samples.

Results

Model validation and fits

During the ICTA, a progression of cell morphology was observed similar to that previously reported for cell spread-

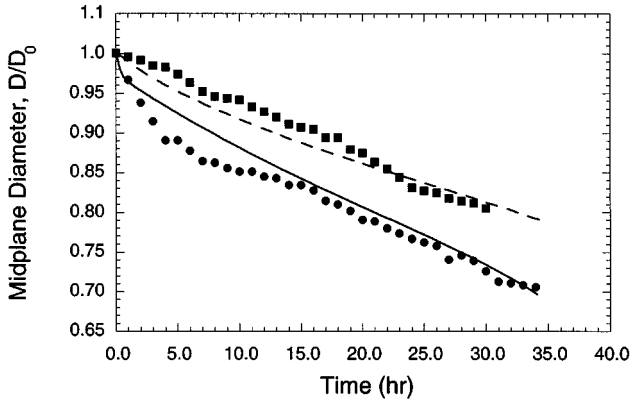

Figure 3. Radial compaction and the effect of TE cylinder aspect ratio.

The circles in the plot show the reduction in diameter of the TE cylinder for HFF at an initial cell concentration, $c_0 =$ 20,000 cells/mL at the midplane (that is, the plane equidistant from the platens), and the solid line represents the fit of the model based on the ABT to the data ($\tau_0 = 0.037$ dyne·cm/cell, $k_{sp} = 1.5$, and $t_{1/2} = 3$ h). The effect of decreasing the aspect ratio (L/D_0) by one-half on midplane compaction was investigated. Using the same value for τ_0 obtained from the fit of the data represented by the circles, the model (dashed line) slightly overpredicted the experimental data (squares), indicating a possible role for network stress modulating cell traction.

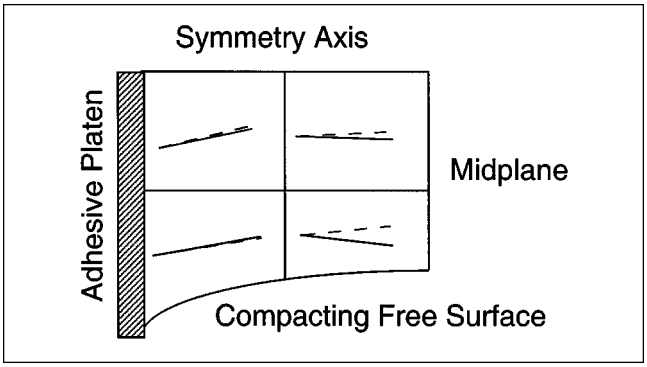

Figure 4. Cell alignment.

HFF alignment measured in the ICTA at 24 h shown by the circles in Figure 3 (solid line) compared favorably with the predicted alignment (dashed lines, calculated from the eigenvalues of Ω_c) based on $\tau_0 = 0.037$ dyne·cm/cell at all positions within the TE cylinder. The corresponding values and standard deviations for the alignment direction are shown in Table 2. The agreement between the model and ICTA data validates the ability of the ABT to capture the anisotropic behavior of compacting TEs.

ing in attached gels (Tomasek and Hay, 1984; Eastwood et al., 1995). Within 2 h, the cells began to extend two or three small protrusions and, within 8 h all the cells had started to elongate into a spindle-like shape (Lee et al., 1993). Cell migration was observed after cell spreading had occurred. However, gel compaction was measurable as early as 30 min. The midplane diameter of a sample prepared with HFF at an initial cell concentration c_0, of 20,000 cells/mL is plotted vs. incubation time as the circles in Figure 3 along with the model fit to the data (solid line). The value for the halftime for

Table 2. HFF Alignment in the ICTA

	Quadrant in ICTA Sideview Projection			
	Bottom Left	Top Left	Bottom Right	Top Right
Avg. Cell Alignment, Exp. ($n = 25$ cells for each quadrant)	$9.0° \pm 6.9°$	$12.9° \pm 6.0°$	$-6.9° \pm 5.5°$	$-1.8° \pm 6.6°$
Avg. Cell Alignment, Simulation	8.8°	11.8°	5.2°	3.2°

spreading for HFF ($t_{1/2}$, which affects the initial part of the compaction curve) was determined to be 3 to 5 h, consistent with measurements of HFF in floating collagen gel (Barocas et al., 1995) with variations being due presumably to differences in cell passage number, variations in cell culture and/or preparation conditions. Values in this range were used in subsequent simulations. The model adequately fits the compaction data both in the early time points (during cell spreading), which depends on the transient value of $\tau_0(t)$ via appropriate values of k_{sp} and $t_{1/2}$, as well as the ultimate value τ_0 (see Eq. 9), and during the period of significant TE compaction, which is determined solely by τ_0. Since the ultimate traction was of primary interest for comparison between groups, τ_0 was the only fitted parameter reported among k_{sp}, $t_{1/2}$, and τ_0.

The model predicts that midplane compaction during the ICTA will decrease for TE cylinders of decreasing aspect ratio (defined as L/D_0). This is mainly due to constrained radial compaction near the adhesive platens at the ends of the TE cylinder, resulting in a reduced extent of radial compaction and reduced network stress for shorter cylinders (Barocas, 1996). In order to test this experimentally, TE

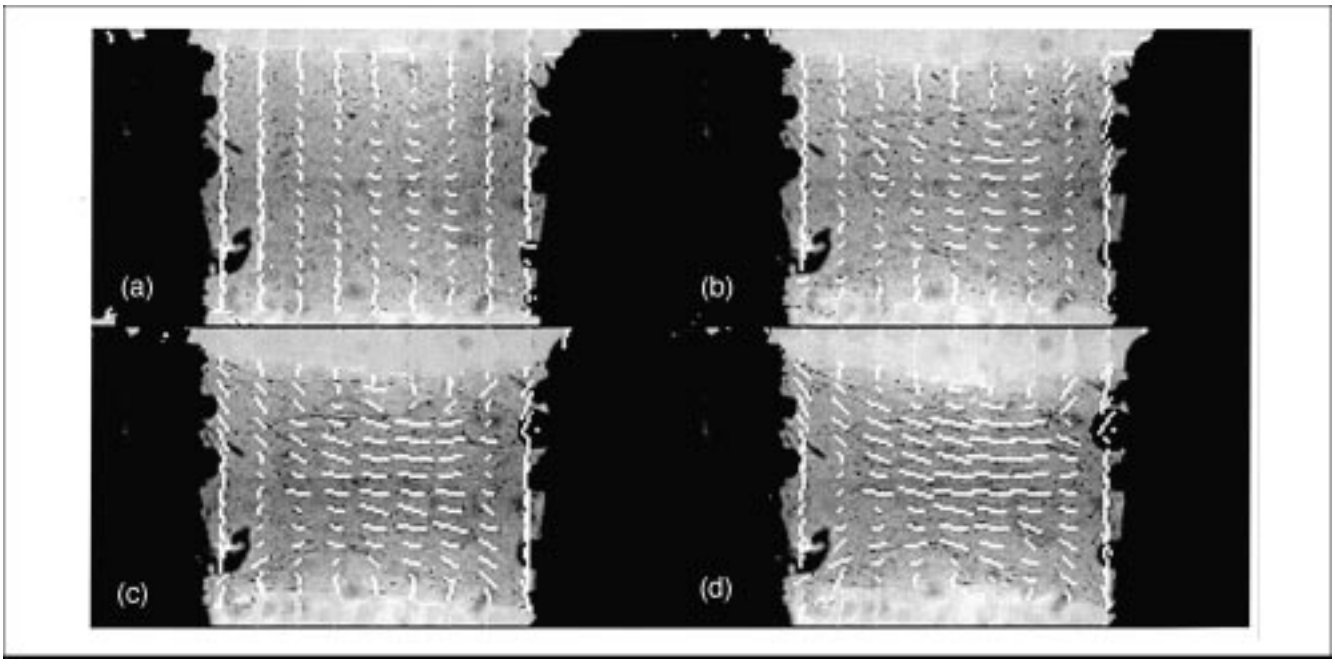

Figure 5. Fibril alignment.

A low magnification polarized light time lapse was used to determine the spatial variation of retardation and thus collagen fibril alignment during the ICTA (images taken at (a) 2, (b) 7, (c) 12, and (d) 17 h). The white lines appear curved in some instances do to a pixelation artifact.

cylinders with L/D_0 one-half that described above were assayed. The measured midplane diameter is shown as the squares in Figure 3. Then, using the value of τ_0 determined from the fit to the data for the standard L/D_0 shown as circles in Figure 3, the experiment was simulated and shown as the dotted line in Figure 3. The simulation slightly overpredicts the extent of compaction for the shorter cylinder at early time points, but adequately predicts the compaction at the end of the experiment. This result, along with similar results for TE tubes with compaction constrained by a mandrel placed in the lumen (Barocas et al., 1998), indicated that developing stress within the collagen network could be a factor in the apparent increase in cell traction and guided our study into the effect of network stress on τ_0, as described in a subsequent section.

Developing cell alignment along the TE cylinder axis with increasing radial compaction is predicted from the model as a result of contact guidance. Fibril alignment develops in the axial direction as a direct result of the radial compaction because the ABT assumes that fibrils align perpendicular to the direction of network compression (and parallel to the direction of network extension) and cells then align with the fibrils. Using the same conditions as for the experiment shown by the circles in Figure 3, cell alignment was measured during the ICTA as a function of position in the TE. Then, we simulated the experiment using the value for τ_0 estimated from the experiment and calculated an average alignment in the TE at the same positions as measured. The experimental and simulated alignment directions are shown as the lines in Figure 4, and the values and their associated standard deviations are reported in Table 2. The reported angles represent the average angle of the long axis of the cell relative to the long axis of the TE cylinder. Because of its axisymmetry, only the values from one quadrant of the projection of the TE cylinder are reported. The simulated values fall within one standard deviation of the experimental data; therefore, the ABT adequately predicted the cell alignment.

A measure of the developing fibril alignment as a function of position in the TE cylinder would serve to further validate the anisotropic aspects of the ABT. To do so, a retardation map of a TE cylinder was generated in time lapse as a function of position in the TE cylinder, since retardation reflects the local axis and strength of fibril alignment (Girton et al., 1998; Guido and Tranquillo, 1993). The results are shown as a series of light micrographs in Figure 5, taken at 2, 7, 12, and 17 h. The angle of the white lines superimposed on the image represents the local axis of fibril alignment (extinction angle) at the midpoint of its location, while the length of the line represents the strength of alignment (retardation). The sample starts out mostly isotropic (except near the platens), as evidenced by the short lengths of the lines. However, as radial compaction ensues, the strength of the fibril alignment increases dramatically in the axial direction, especially near the midplane of the ICTA where the compaction is greatest, while the fibril alignment remains largely isotropic near the axis towards the platens where little compaction occurs (except towards the edge of the platens, as predicted (Barocas and Tranquillo, 1997b)). The observed decrease in retardation δ with increasing radius in the TE cylinder reflects the decreased thickness of collagen gel in the optical path λ rather than indicating decreased alignment of collagen fibrils towards the surface of the TE cylinder. This would be apparent in a map of birefringence δ/λ.

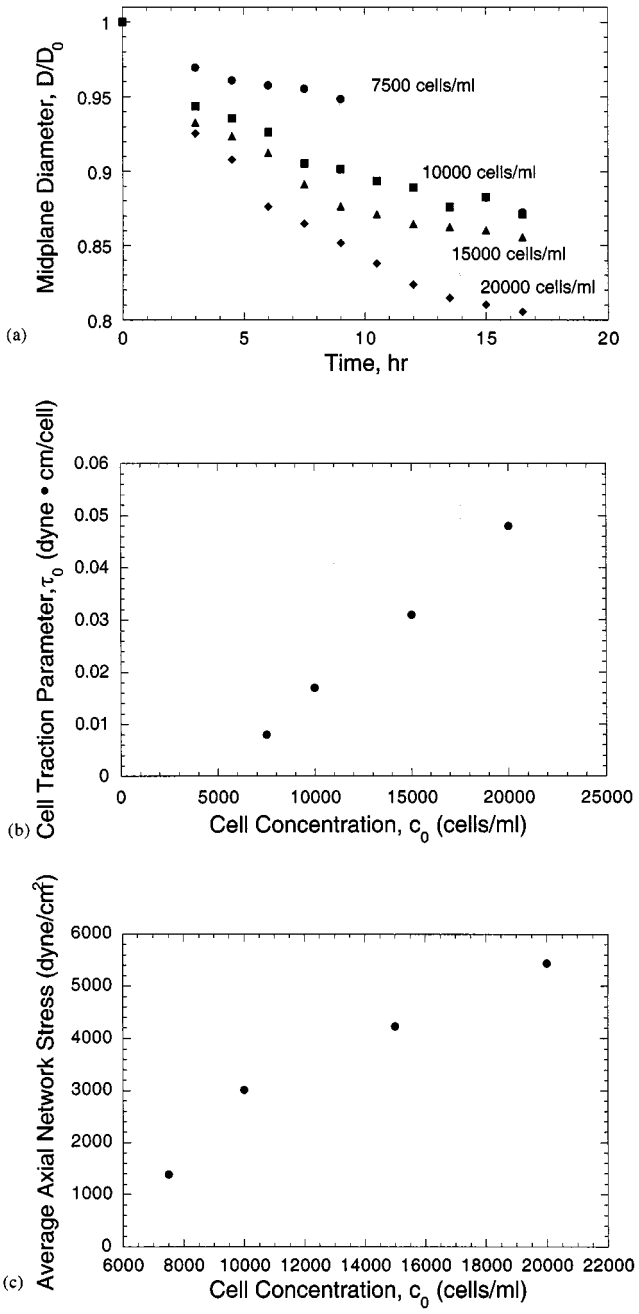

Figure 6. Cell concentration effect.

Increasing midplane compaction with increasing c_0 is shown in (a). The resulting τ_0 from model fits to the compaction curves are shown in (b), with increasing estimated τ_0 with increased c_0. (c) A possible explanation for this is increased network stress signaling an increase in cell traction, the average axial stress at 16 h being plotted for increased c_0.

Effect of cell concentration

To determine the effect of cell concentration (and thus increasing radial compaction and stress) on cell traction, we varied c_0 from 7,500 to 20,000 cells/mL in the ICTA and measured midplane compaction, as shown in Figure 6a. Be-

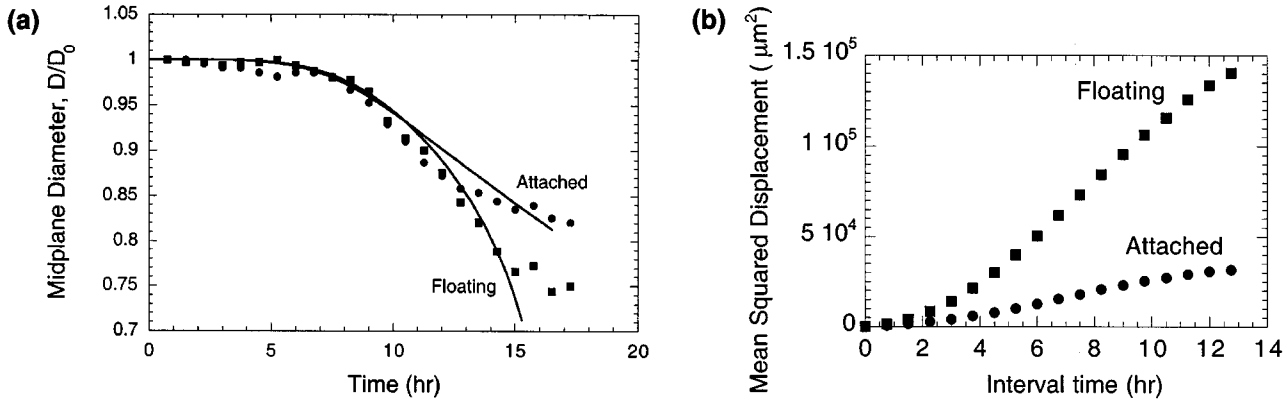

Figure 7. Network stress effect.

HFF within attached, mechanically stressed TEs (ICTA) exerted 25% more traction (a) but exhibited much decreased migration (b) than within floating TEs. Although the floating TE compacted radially to a greater extent than the attached TE, the estimated value of τ_0 is lower (see text for explanation).

low 7,500 cells/mL, HFF spreading was delayed considerably and the cell number within the ICTA was not sufficient to compact the collagen gel within the 16 h period of experiment. Above 20,000 cells/mL, the network strain typically associated with compaction after 16 h was significantly over the 15% value for the linear viscoelastic limit of collagen gel (Knapp et al., 1997) and invalidated Eq. 7. Values of τ_0 estimated from fitting these data for each c_0 are shown in Figure 6b. As c_0 increased, the extent of compaction increased as seen in Figure 6a, thus resulting in even higher cell and collagen concentrations in the highly compacted regions with correspondingly higher network stress, as shown by the simulated spatial averaged axial stress in the network in Figure 6c. As seen in Figure 6b, τ_0 increased significantly with increasing c_0 as did the network stress, indicating a possible correlation between increased network stress (to which the cells are subject) and increased cell traction.

Effect of network stress on HFFs: ICTA vs. floating TE cylinders

Compaction in the ICTA and in a floating TE cylinder prepared in the same experiment is shown in Figure 7a, along with the model fits for both cases. Even though ICTA compaction was slightly less than that for the floating cylinder, the value for τ_0 was 25% greater (statistically significant, $P < 0.05$). This was due to axial alignment of collagen fibrils and cells in the ICTA, causing an increasing amount of traction to be directed axially, reducing radial compaction (c.f. Introduction) which was ''compensated'' for in the fitting by using a greater τ_0. However, cell migration was significantly higher in the floating cylinder ($P < 0.05$), as shown in Figure 7b, indicating negatively correlated cell traction and migration. Results are summarized in Table 3.

Table 3. Effect of Network Stress on HFFs

Parameter	Attached Gel Control Stressed	Floating Gel Stress-Free
Migration $\mathfrak{D}_0$ (μm^2/min)	7.41 ± 1.35 ($n = 10$)	$^*38.7 \pm 10.8$ ($n = 6$)
Traction τ_0 (dyne·cm/cell)	0.115 ± 0.011 ($n = 10$)	$^*0.083 \pm 0.011$ ($n = 6$)

*Statistically significant difference ($P < 0.05$).

Effect of modulating HFF adhesion with a blocking anti-β_1 integrin antibody

The ICTA was conducted with medium containing human anti-β_1 integrin antibody, which is known to modulate the adhesion of HFF to collagen gels and collagen gel compaction (Carver et al., 1995). Anti-β_1 was added at 2 μg/mL, which still allowed cell spreading, but modulated the traction and migration of the HFF. Light micrographs of a typical HFF in collagen gel in the presence and absence of anti-β_1 are shown in Figures 8a and 8b. The morphology of many of the cells in the presence of anti-β_1 (more polarized appearance, with large protrusions in the direction of migration) was also typical for those cells in the absence of anti-β_1 observed to be more actively migrating; in contrast, relatively stationary fibroblasts appeared hyperelongated with long thin protrusions at both ends and lacked distinguishable polarity. Anti-β_1 in the culture medium at a concentration of 2 μg/mL resulted in significantly decreased compaction, and significantly increased migration ($P < 0.05$). Results are summarized in Table 4.

Effect of stimulating RDF with PDGF-BB

In order to further investigate the relationship between cell traction and migration, PDGF-BB was added to the culture medium in studies using RDFs since it was found to enhance RDF, but not HFF migration within collagen gel (unpublished observations). A comparison of the midplane compaction and migration with and without 50 ng/mL PDGF-BB was performed. As observed for the anti-β_1 antibody, there existed a negative correlation between migration and traction in the PDGF-BB treated samples, where elevated PDGF-BB increased $\mathfrak{D}_0$ significantly but decreased τ_0 ($P < 0.05$). Results are summarized in Table 5. If cell proliferation had increased with the addition of PDGF-BB beyond that accounted for with the value used for k_0, the fitted values of τ_0

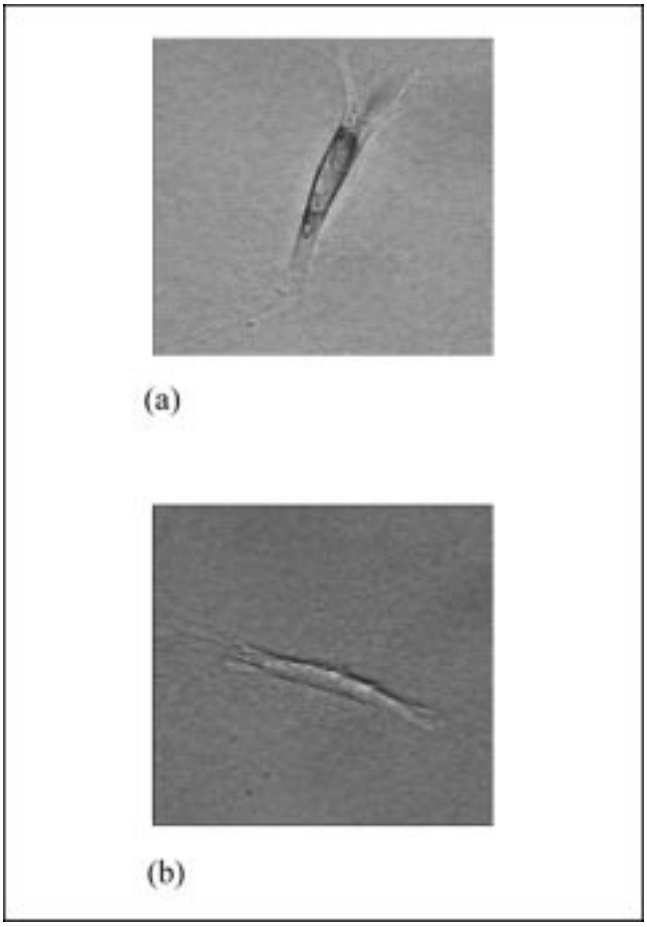

Figure 8. Increased polarity of migrating fibroblasts.

High magnification micrographs of typical migrating (a) and relatively stationary (b) HFF as directly observed in time-lapse. The cell in (a) was migrating toward the top of the image.

would have decreased further in order to compensate for the increased cell concentrations, consistent with a more negative correlation.

Discussion

We have presented results from an ICTA assay for measuring cell traction and migration. We have also validated the ability of our ABT model to simulate ICTA data by predicting the spatial dependence of alignment of fibroblasts and collagen fibrils in the compacting TE cylinder and the effects of aspect ratio on compaction. The effects of migration stimulating and adhesion modulating factors (PDGF-BB and an anti-β_1 integrin antibody), as well as the collagen network mechanical stress state (attached vs. floating TE cylinders) on cell migration and traction during compaction were investigated, and, in all cases, cell migration was negatively correlated with cell traction. While this may have been anticipated from studies based on the degree of traction wrinkles developed on rubber films for fast (less wrinkles) and slow (more wrinkles) migrating cell types (Harris et al., 1980), it has never been shown in a tissue-like environment.

The cylindrical geometry of our ICTA was motivated by our ability to model the system using a 2-D axisymmetric model for TEs (Barocas and Tranquillo, 1997b) based on our ABT (Barocas and Tranquillo, 1997a), but also conferred other advantages compared to previously reported ICTAs. A key advantage results from our estimation of traction based on TE compaction rather than direct force measurement. Direct force measurement by attaching a force transducer to a TE (Delvoye et al., 1991; Kolodney and Wysolmerski, 1992; Eastwood et al., 1994) precludes the possibility of comparing traction exerted by cells in attached (stressed) and floating (stress-free) TEs. Another advantage is the small volume of our assay minimizes the costs of studying the effect of expensive soluble factors such as growth factors or neutralizing antibodies on the cell behavior in the TE (only about 30 μL of collagen suspension is required for the TE, and about 1 mL incubation medium is required to fill the assay chambers). Other reported ICTAs which rely on direct force measurement require larger samples to generate measurable forces. The design of our ICTA allowed the TE to be directly viewed on the inverted microscope. This ability to monitor compaction of the TE at low magnification while simultaneously tracking the cells with high precision at high magnification was instrumental to the study of the relationship between cell migration and traction, minimizing variability due to differences in preparations of cells and collagen gel between experiments.

It was obvious from direct observation of the ICTA under low magnification that cell movement due to TE compaction was significant in comparison to the cell migration, especially at high cell concentrations. By tracking marker beads, which also convected with the compacting TE near to the cells under observation, we effectively corrected for this, as evidenced by our measurement of negligible migration for immotile rounded cells during the time lapse (data not shown). However, in cases with extensive cell migration, the possibility existed that the cells would migrate significantly from the marker bead chosen for it during the later stages of the time

Table 4. Effect of 2 μg/mL Anti-β_1 Integrin Antibody Added to the ICTA Medium on HFFs

Parameter	Anti-β_1 Control	+ Anti-β_1
Migration $\mathfrak{D}_0$ (μm^2/min)	4.05 ± 0.51 ($n = 9$)	$^*6.45 \pm 0.66$ ($n = 8$)
Traction τ_0 (dyne·cm/cell)	0.084 ± 0.006 ($n = 9$)	$^*0.020 \pm 0.002$ ($n = 8$)

*Statistically significant difference ($P < 0.05$).

Table 5. Effect of 50 ng/mL PDGF-BB Added to the ICTA Medium on RDFs

Parameter	PDGF-BB Control	+ PDGF-BB
Migration $\mathfrak{D}_0$ (μm^2/min)	3.54 ± 0.30 ($n = 6$)	$^*4.89 \pm 0.36$ ($n = 6$)
Traction τ_0 (dyne·cm/cell)	0.135 ± 0.01 ($n = 6$)	$^*0.055 \pm 0.007$ ($n = 6$)

*Statistically significant difference ($P < 0.05$).

lapse, so that the accuracy of the correction would worsen considerably since the compaction in the ICTA is spatially nonuniform. In order to minimize this problem, in cases where cell migration was measured, cell concentrations were limited to 1.25×10^4 cells/mL, a relatively low cell concentration that allowed for significant generation of axial stress in the ICTA over the course of the experiment, but was low enough that the maximum strain (at the ICTA midplane) was limited to about 10% at the end of the experiment.

The ICTA proved to be a valuable tool in validating some of the basic assumptions of the ABT, which had previously been validated in floating TE spheres (Barocas et al., 1995) and constrained TE tubes (Barocas et al., 1998). As shown in Figure 2, the shape of the compaction curves were approximated well with a three parameter fit for cell spreading (k_{sp} and $t_{1/2}$) and cell traction (τ_0), with all other model parameters determined experimentally in separate experiments. In addition, the ability of the model to predict axial cell alignment in the ICTA (Figure 4 and Table 2) was important, since the increasing axial alignment of fibroblasts within the ICTA had important effects on both the axial stress and radial compaction of the ICTA. In the ABT, cells are assumed to exert stress in the direction in which they are aligned as measured by the cell contact guidance sensitivity parameter κ. This assumption results in increased axial stress and reduced radial compaction predicted for $\kappa > 0$, which was responsible for the greater value for τ_0 required to fit the ICTA data in Figure 7a despite compaction being greater in the floating TE cylinder. The functionality of the contact guidance terms in the ABT (see Eqs. 4—6) that was used to estimate $\kappa = 4$ from confined compression of TEs (Girton et al., 1999) was thus validated for cell traction induced TE compaction in the ICTA, a result also reported for compacting TE tubes (Barocas et al., 1998).

The measurement of developing axial alignment of collagen fibrils in the ICTA in areas of high radial compaction (Figure 5) was further indication of the validity of the anisotropic aspects of the ABT. To our knowledge, this is the first report of direct *in-situ* measurement of developing fibril alignment in TEs. In addition to providing a valuable tool for directly studying contact guidance fields within compacting TEs, which could be useful for studying developing alignment in TEs with application to tissue engineering (Barocas et al., 1998), the methods used to obtain the time-lapse images shown in Figure 5 have been invaluable for studying the process by which collagen gels align under external fields (Tower and Tranquillo, 1999).

Another prediction of the ABT is decreased compaction and network stress in the ICTA for cylinders with a lower aspect ratio L/D_0. Indeed, the experimental data in Figure 3 showed that compaction of the ICTA was reduced for a cylinder with an aspect ratio which was halved. However, using the same parameter values as was used in the simulation for the data with larger aspect ratio in Figure 3, the simulated compaction curve significantly overpredicted the ICTA compaction, especially during the first 15 h of the experiment. This indicated there might be a correlation between increasing compaction (and therefore network stress) and increased cell traction measured as τ_0. Grinnell and colleagues have shown that fibroblasts respond to mechanical stress in TEs with a change in phenotype, with increased proliferation, biosynthesis, and highly elongated morphology in other attached TEs in which mechanical stress also develops. In contrast, fibroblasts have a relatively quiescent phenotype in floating, essentially stress-free TEs (Nakagawa et al., 1989) in which the cell traction stress is balanced by the network viscoelasticity (Barocas and Tranquillo, 1997a). Importantly, the relaxation of stressed TEs results in the disappearance of actin stress fibers in fibroblasts and release of cell surface fibronectin (Tomasek and Hay, 1984; Mochitate et al., 1991), both of which are factors that could significantly affect the way the fibroblasts exert traction and migrate within the TEs. The results of Figure 7 and Table 3 indicating increased cell traction in attached (stressed) TEs were consistent with these observations. That is, fibroblasts that are strongly adherent to the collagen, possibly via cell surface fibronectin with prominent actin stress fibers, efficiently compact the local network but do not migrate efficiently, while the fibroblasts within the floating unstressed TE channel a reduced level of traction into efficient migration.

Our traction and migration results for attached and floating TEs (Figure 7) indicated a negative correlation between migration and traction associated with a difference in the mechanical stress state of the network. Recently, Lauffenburger and coworkers reported a negative correlation between migration and adhesion strength for fibroblasts on a 2-D substratum, where fibroblasts migrated faster as adhesion was increased from a low level, but slower as adhesion increased above an optimal level (Palacek et al., 1997). Our results of increased HFF migration treated with blocking anti-β_1 integrin antibody suggest that HFF in the TE were strongly adherent to the collagen network in the absence of the antibody, but were able to migrate more efficiently when adhesion was decreased in the presence of the antibody (Table 4). This increase in migration efficiency was correlated with a more polar fibroblast morphology that may have facilitated migration. The concomitant decrease in compaction suggested that the strongly adherent cells, while less efficient in migrating, were more efficient in exerting traction (Table 4). Similarly, upon the addition of PDGF-BB to ICTAs prepared with RDF, increased migration was measured, again along with negative correlation with (decreased) cell traction (Table 5).

The negative correlation between migration and traction that we have documented for TEs has implications towards understanding the role of fibroblasts in wound repair, where an increased state of mechanical stress in the wound may result from wound contraction driven by wound fibroblasts. Upon wounding, chemokines and chemoattractants such as growth factors and ECM fragments are released in the wound, inducing progenitor cells of the wound fibroblasts (such as quiescent dermal fibroblasts (Clark, 1996) or pericytes (Ivarsson et al., 1996)) to become migratory, invading the fibrin clot. The negative correlation between migration and traction is inconsistent with speculation that cell migration provides the driving force for wound contraction. In fact, if stress begins to develop within the wound site due to the invading fibroblasts, our results indicating increased traction and decreased migration of cells in mechanically stressed TEs suggests the now resident wound fibroblasts would exert enhanced traction, perhaps associated with expression of α-smooth muscle actin typical of myofibroblasts (Gabbiani et

al., 1971). Their decreased migration correlating with increased traction would keep them localized within the wound. Further, factors that modulate this negative correlation of cell behavior might be antagonist to the outcome of wound contraction. Our results in the ICTA (where stress develops) for PDGF-BB, which is likely present in relatively high concentrations within the wound initially, suggest that growth factors might counteract this effect of stress since PDGF-BB caused traction to decrease and migration to increase. A similar scenario follows from our ICTA results using the anti-β_1 integrin antibody given the increase in soluble ECM fragments associated with clot resorption that could compete with the developing granulation tissue for cell integrins and thereby cause traction to decrease. Thus, the degree of wound contraction likely depends in a complex way on the spatiotemporal characteristics of mechanical stress and concentration of growth factors, ECM, and soluble ECM fragments within and around the wound.

Acknowledgments

This work has been supported by NIH P01-GM50150-03S1 (RTT) and NSF Research Training grant BIR-9413241 (DMK). The technical assistance of Cynthia Coulter, David Bleckinger, Andy Lenneman, and Sam Kean and helpful discussions with David Shreiber, Narendra Dubey, and Paul Enever are gratefully acknowledged.

Literature Cited

Barocas, V. H., ''Anisotropic Biphasic Modeling of Cell-Collagen Mechanical Interactions in Tissue Equivalents,'' PhD Thesis, Univ. of Minnesota (1996).

Barocas, V. H., T. S. Girton, and R. T. Tranquillo, ''Engineered Alignment in Media-Equivalents: Magnetic Prealignment and Mandrel Compaction,'' *J. Biomech. Eng.*, **120**, 660 (1998).

Barocas, V. H., A. G. Moon, and R. T. Tranquillo, ''The Fibroblast-Populated Collagen Microsphere Assay of Cell Traction Force: 2. Measurement of the Cell Traction Parameter,'' *J. Biomech. Eng.*, **117**, 161 (1995).

Barocas, V. H., and R. T. Tranquillo, ''Biphasic Theory and *in vitro* Assays of Cell-Fibril Mechanical Interactions in Tissue-Equivalent Collagen Gels,'' *Cell Mechanics and Cellular Engineering*, V. C. Mow, F. Guilak, R. Tran-Son-Tay, and R. M. Hochmuth, eds., Springer-Verlag, New York, p. 185 (1994).

Barocas, V. H., and R. T. Tranquillo, ''An Anisotropic Biphasic Theory of Tissue-Equivalent Mechanics: the Interplay Among Cell Traction, Fibrillar Network Deformation, Fibril-Alignment, and Cell Contact Guidance,'' *J. Biomech. Eng.*, **119**, 137 (1997a).

Barocas, V. H., and R. T. Tranquillo, ''A Finite Element Solution for the Anisotropic Biphasic Theory of Tissue-Equivalent Mechanics: the Effect of Contact Guidance on Isometric Cell Traction Measurement,'' *J. Biomech. Eng.*, **119**, 261 (1997b).

Bell, E., B. Ivarsson, and C. Merrill, ''Production of a Tissue-Like Structure by Contraction of Collagen Lattices by Human Fibroblasts of Different Proliferative Potential *in vitro*,'' *Proc. Nat. Acad. Sci. U.S.*, **76**, 1274 (1979).

Bromberek, B. A., D. M. Knapp, P. A. J. Enever, M. D. Caldwell, and R. T. Tranquillo, ''The Fibroblast Populated Microsphere Wound Healing Assay. Use of Controlled Release of GRGDSP to Elicit Chemotaxis,'' in press (1999).

Brown, A. F., ''Neutrophil Granulocytes: Adhesion and Locomotion on Collagen Substrata and in Collagen Matrices,'' *J. Cell Sci.*, **58**, 455 (1982).

Carver, W., I. Molano, T. A. Reaves, T. K. Borg, and L. Terracio, ''Role of the Alpha 1 Beta 1 Integrin Complex in Collagen Gel Contraction *in vitro* by Fibrobasts,'' *J. Cell Phys.*, **165**, 425 (1995).

Clark, R. A. F., ''Wound Repair: Overview and General Considerations,'' *The Molecular and Cellular Biology of Wound Repair*, R. A. F. Clark and P. M. Henson, eds., Plenum, New York, p. 3 (1996).

Delvoye, P., P. Wiliquet, J. L. Leveque, B. Nusgens, and C. Lapiere, ''Measurement of Mechanical Forces Generated by Skin Fibroblasts Embedded in a Three-Dimensional Collagen Gel,'' *J. Invest. Dermatol.*, **97**, 898 (1991).

Dickinson, R. B., S. Guido, and R. T. Tranquillo, ''Biased Cell Migration of Fibroblasts Exhibiting Contact Guidance in Oriented Collagen Gels,'' *Ann. Biomed. Eng.*, **22**, 342 (1994).

Dickinson, R. B., J. B. McCarthy, and R. T. Tranquillo, ''Quantitative Characterization of Cell Invasion *in vitro*: Formulation and Validation of a Mathematical Model of the Collagen Gel Invasion Assay,'' *Ann. Biomed. Eng.*, **21**, 679 (1993).

Dickinson, R. B., and R. T. Tranquillo, ''Optimal Estimation of Cell Movement Indices from the Statistical Analysis of Cell Tracking Data,'' *AIChE J.*, **39**, 1995 (1993).

Eastwood, M., D. A. McGrouther, and R. A. Brown, ''A Culture Force Monitor for Measurement of Contraction Forces Generated in Human Dermal Fibroblast Cultures: Evidence for Cell-Matrix Mechanical Signalling,'' *Biochim. et Biophys. Acta.*, **1201** 186 (1994).

Eastwood, M., R. Porter, U. Khan, G. McGrouther, and R. Brown, ''Quantitative Analysis of Collagen Gel Contractile Forces Generated by Dermal Fibroblasts and the Relationship to Cell Morphology,'' *J. Cell. Phys.*, **166**, 33 (1995).

Ehrlich, H. P., and J. B. Rajaratnam, ''Cell Locomotion Forces Versus Cell Contraction Forces for Collagen Lattice Contraction: an in vitro Model of Wound Contraction,'' *Tissue Cell.*, **22**, 407 (1990).

Enever, P. A. J., and R. T. Tranquillo, ''PDGF-BB Increases Rat Dermal Fibroblast Migration Within Collagen Gel,'' in press (1999).

Freshney, R. I., *Culture of Animal Cells: A Manual of Basic Technique (2nd Edition)*, Alan R. Liss, Inc., New York (1987).

Gabbiani, G., G. B. Ryan, and G. Majno, ''Presence of Modified Fibroblasts in Granulation Tissue and their Possible Role in Wound Contraction,'' *Experientia*, **27**, 549 (1971).

Girton, T. S., and R. T. Tranquillo, ''Reorientation and Alignment of Collagen Fibrils and Tissue Cells in Confined Compression of a Tissue-Equivalent,'' in press (1999).

Girton, T. S., N. Dubey, and R. T. Tranquillo, ''Magnetic Induced Alignment of Collagen Fibrils in Tissue-Equivalents,'' *Methods in Tissue Engineering*, J. Morgan, ed., Humana Press, Totowa, NJ (1998).

Grinnell, F., and C. R. Lamke, ''Reorganization of Hydrated Collagen Lattices by Human Skin Fibroblasts,'' *J. Cell. Sci.*, **66**, 51 (1984).

Gross, J., W. Farinelli, P. Sadow, R. Anderson, and R. Bruns, ''On the Mechanism of Skin Wound ''Contraction'': a Granulation Tissue ''Knockout'' with a Normal Phenotype,'' *Proc. Nat. Acad. Sci. U. S.*, **92**, 5982 (1995).

Guido, S., and R. T. Tranquillo, ''A Methodology for the Systematic and Quantitative Study of Cell Contact Guidance in Oriented Collagen Gels: Correlation of Fibroblast Orientation and Gel Birefringence,'' *J. Cell. Sci.*, **105**, 317 (1993).

Harris, A. K., P. Wild, and D. Stopak, ''Silicone Rubber Substrata: a New Wrinkle in the Study of Cell Locomotion,'' *Science*, **208**, 177 (1980).

He, Y., and F. Grinnell, ''Stress Relaxation of Fibroblasts Activates a Cyclic AMP Signaling Pathway,'' *J. Cell. Biol.*, **126**, 457 (1994).

Ivarsson, M., C. Sundberg, N. Farrokhnia, H. Pertoft, K. Rubin, and B. Gerdin. ''Recruitment of Type I Collagen Producing Cells from the Microvasculature in vitro,'' *Exp. Cell. Res.*, **229**, 336 (1996).

Knapp, D. M., V. H. Barocas, A. G. Moon, K. Yoo, L. R. Petzold, and R. T. Tranquillo, ''Rheology of Reconstituted Type I Collagen Gel in Confined Compression,'' *J. Rheol.*, **41**, 971 (1997).

Knapp, D. M., E. F. Helou, and R. T. Tranquillo, ''A Fibrin and Collagen Gel Assay for Fibroblast Chemotaxis: Assessment of Chemotaxis to GRGDSP,'' *Exp. Cell. Res.*, **247**, 543 (1999).

Kolodney, M. S., and R. B. Wysolmerski, ''Isometric Contraction by Fibroblasts and Endothelial Cells in Tissue Culture: a Quantitative Study,'' *J. Cell. Biol.*, **117**, 73 (1992).

L'Heureux, N., L. Germain, R. Labbe, and F. A. Auger, ''In vitro Construction of a Human Blood Vessel from Cultured Vascular Cells: a Morphologic Study,'' *J. of Vasc. Surg.*, **17**, 499 (1993).

Lackie, J. M., *Cell Movement and Cell Behavior*, Allen and Unwin, London (1986).

Lee, T. L., Y. C. Lin, K. Mochitate, and F. Grinnell, ''Stress-Relaxation of Fibroblasts in Collagen Matrices Triggers Ectocytosis of Plasma Membrane Vesicles Containing Actin, Annexins II and VI, and Beta 1 Integrin Receptors,'' *J. Cell. Sci.*, **105**, 167 (1993).

Mochitate, K., P. Pawelek, and F. Grinnell, ''Stress Relaxation of Contracted Collagen Gels: Disruption of Actin Filament Bundles, Release of Cell Surface Fibronectin, and Down-Regulation of DNA and Protein Synthesis,'' *Exp. Cell. Res.*, **193**, 198 (1991).
Moon, A. G., ''Cell Traction Forces Exerted on the Extracellular Matrix: Modeling and Measurement,'' PhD Thesis, University of Minnesota (1992).
Murray, J. D., G. F. Oster, and A. K. Harris, ''A Mechanical Model for Mesenchymal Morphogenesis,'' *J. Math. Biol.*, **17**, 125 (1983).
Nakagawa, S., P. Pawelek, and F. Grinnell, ''Extracellular Matrix Organization Modulates FIbroblast Growth and Growth Factor Responsiveness,'' *Exp. Cell Res.*, **182**, 572 (1989).
Olsen, L., J. A. Sherratt, and P. K. Maini, ''A Mechanochemical Model for Adult Dermal Wound Contraction and the Permanence of the Contracted Tissue Displacement Profile,'' *J. of Theor. Biol.*, **177**, 113 (1995).
Oster, G. F., J. D. Murray, and A. K. Harris, ''Mechanical Aspects of Mesenchymal Morphogenesis,'' *J. Embryol Exp. Res.*, **78**, 83 (1983).
Palacek, S. P., J. C. Loftos, M. H. Ginsberg, D. A. Lauffenburger, and A. F. Horwitz, ''Integrin-Ligand Binding Properties Govern Cell Migration Speed through Cell-Substratum Adhesiveness,'' *Nature*, **385**, 537 (1997).
Scherer, G. W., S. A. Pardenek, and R. M. Swiatek, ''Viscoelasticity in Silica Gel,'' *J. of Non-Crystalline Solids*,**108**, 14 (1988).
Schmalstieg, F. C., H. E. Rudloff, G. R. Hillman, and D. C. Anderson, ''Two-Dimensional and Three-Dimensional Movement of Human Polymorphonuclear Leukocytes: Two Fundamentally Different Mechanisms of Locomotion,'' *J. Leuk Biol.*, **40**, 677 (1986).
Tomasek, J. J., and E. D. Hay, ''Analysis of the Role of Microfilaments and Microtubules in Acquisition of Bipolarity and Elongation of Fibroblasts in Hydrated Collagen Gels,'' *J. Cell. Biol.*, **99**, 536 (1984).
Tower, T. T., and R. T. Tranquillo, ''Alignment Maps in Tissues and Fibrillar Materials/Revisiting Old Polarized Light Methods with Current Technology,'' in press (1999).
Tranquillo, R. T., and J. D. Murray, ''Continuum Model of Fibroblast-Driven Wound Contraction: Inflammation-Mediation,'' *J. Theor. Biol.*, **158**, 135 (1992).
Tuan, T. L., A. Song, S. Chang, S. Younai, and M. E. Nimni, ''In vitro Fibroplasia: Matrix Contraction, Cell Growth, and Collagen Production of Fibroblasts Cultured in Fibrin Gels,'' *Exp. Cell Res.*, **223**, 127 (1996).

Manuscript received Feb. 15, 1999, and revision received July 19, 1999.